ISSN 1990-7931, Russian Journal of Physical Chemistry B, 2013, Vol. 7, No. 1, pp. 35–43. © Pleiades Publishing, Ltd., 2013.
Original Russian Text © S.M. Frolov, A.V. Dubrovskii, V.S. Ivanov, 2013, published in Khimicheskaya Fizika, 2013, Vol. 32, No. 2, pp. 56–65.

COMBUSTION, EXPLOSION, AND SHOCK WAVES

Three-Dimensional Numerical Simulation of the Operation of a Rotating-Detonation Chamber with Separate Supply of Fuel and Oxidizer

S. M. Frolov, A. V. Dubrovskii, and V. S. Ivanov

Semenov Institute of Chemical Physics, Russian Academy of Sciences, Moscow, Russia

e-mail: smfrol@chph.ras.ru

Received April 12, 2012

Abstract—A three-dimensional numerical simulation of the operation of an annular rotating-detonation chamber (RDC) with separate supply of combustible mixture components, hydrogen and air, is performed, and the calculation results are compared to available experimental data. The model is based on a system of time-dependent Reynolds-averaged Navier–Stokes equations complemented with a turbulence model and continuity and energy equations for a multicomponent reacting gas mixture. The system is solved using a coupled algorithm based on the finite volume method and particle method. Calculations are for the first time performed with allowance for effects of finite rates of turbulent and molecular mixing of the combustible mixture components with each other and with reaction and detonation products. The calculation results compare favorably with the experimental data obtained at the Lavrentyev Institute of Hydrodynamics of the Siberian Branch of the Russian Academy of Sciences.

Keywords: rotating-detonation chamber, multidimensional numerical simulation, comparison with experiment

DOI: 10.1134/S1990793113010119

INTRODUCTION

At present, power plants in aircraft are mainly turbine engines (GTEs), operating according to the Brayton thermodynamic cycle. The same cycle is widely used in rocket engines, in particular in liquid propellant rocket engines (LPREs). For many decades, GTEs and LPREs have been continually improved, and further progress in this direction is possible only with extensive use of expensive new technologies and heat-resistant materials. One alternative that potentially can significantly enhance the thermodynamic efficiency of modern GTEs and rocket engines is the use of combustion chambers with an increased total pressure. The total pressure in the combustion chamber can be increased by intensifying the combustion of the fuel–oxidizer mixture and/or by changing the mode of combustion. The most advantageous mode (from the point of view of thermodynamic efficiency) is detonation [1, 2]. In a detonation wave, the maximum concentration of the chemical energy stored in the fuel is achieved: energy is released in a thin layer of shock-compressed mixture. Two basic schemes of detonation are known [3]: periodic detonation waves propagating along the combustion chamber (pulse detonation chamber), and detonation waves continuously circulating in the tangential direction around the combustion chamber (rotating-detonation chamber RDC). Both schemes are considered promising for rocket and air-breathing jet engines. This work is a continuation of [4], where we examined the possibility of integrating the RDC into the GTE.

For accurate simulation, optimization, and determination of the region of stable operation of the RDC, the mathematical model should be carefully tested by comparing its predictions with experimental data. In what follows, we describe the results of numerical simulations of the rotating detonation of a hydrogen–air mixture in an annular flow chamber with the same design and dimensions as that described in [5, 6]. In contrast to all known computational studies (see, e.g., [4, 7, 8]), we for the first time simulate the operation of a RDC with separate fuel and oxidizer supply.

ROTATING-DETONATION CHAMBER

Figure 1 shows a diagram of the rotating-detonation chamber and the sizes of its key elements. The combustion chamber appears to be an axisymmetric annular channel with an internal and external diameters of the annular gap of $d_{int} = 260$ mm and $d_{ext} = 306$ mm, respectively (with gap width of $\Delta = 23$ mm) and a length of $z = L_c = 400$ mm. The axial distance is measured from the RDC bottom ($z = 0$). Between the bottom and the outer wall of the chamber, there is an annular slit of width $\delta = 2$ mm for supply of gaseous

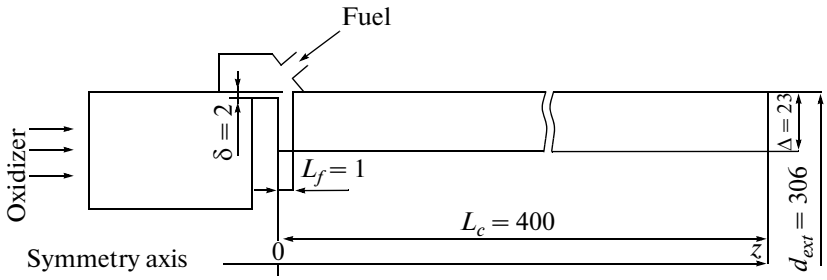

Fig. 1. Dimensions (in mm) of the rotating detonation chamber.

oxidizer in the axial direction from an oxidizer collector. Fuel enters the chamber from a fuel collector in the radial direction through holes evenly spaced over the circumference of the chamber's outer wall $z = L_f =$ 1 mm apart. The total cross-sectional area of the holes is $S_f = 0.4$ cm^2. The right end of the RDC is open to the environment.

MATHEMATICAL MODEL

The physicochemical processes in the RDC were simulated using the mathematical model described in detail in [4]. Here, we limit ourselves to a brief description of its main features.

The flow of a viscous compressible gas in the RDC was described using the three-dimensional time-dependent Reynolds-averaged Navier–Stokes, energy, and species conservation equations for a multicomponent mixture. The turbulent fluxes of species, momentum, and energy were modeled within the framework of the standard k–ε turbulence model. Given that all physicochemical processes in the RDC occur in a very short time, the contribution from the frontal (laminar and/or turbulent) combustion to the chemical sources in the equations of conservation of energy and components of the mixture was neglected. The contributions of these reactions to the indicated bulk chemical sources were determined using the particle method (PM) [9–12, 4].

The most important advantage of the PM is its ability to accurately determine the rates of chemical reactions in a turbulent flow without invoking any hypothesis about the influence of turbulent fluctuations of the temperature and concentrations of the reactants on the mean rate of the reaction. In the PM algorithm, the instantaneous local states of a turbulent reacting flow are represented as a set of interacting (Lagrangian) particles. Each particle has its individual properties: the position in space, three velocity components, volume, density, temperature, mass fractions of chemical components, and statistical weight, which is used to determine the mean values of the variables over the ensemble of particles. For each particle, the system of equations of conservation of mass of the species, momentum, and energy is solved; the flux (transfer) terms are calculated using the classic models of linear relaxation to the mean [9] The equations of the model were closed by the caloric and thermal equations of state of a mixture of ideal gases with variable heat capacity, as well as by the initial and boundary conditions. All the thermophysical parameters of the gas were considered variable.

METHOD OF CALCULATION AND BASIC PARAMETERS

Numerical solution of the governing equations of the problem was carried out using the coupled algorithm "SIMPLE method [19]–Monte Carlo method". The chemical sources were calculated by an implicit scheme with an internal time step of integration. The coupled algorithm was previously used to simulate flame acceleration and deflagration-to-detonation transition in smooth tubes and in tubes with obstacles [11, 12], as well as to solve the problems of shock-initiated autoignition and preflame ignition in confined spaces [14]. In all cases, satisfactory agreement between the results of calculations and experiments were observed. In addition, this algorithm was used to solve the problem of the limits of existence of detonation in the RDC operating on homogeneous hydrogen–air mixture.

As in [4], in the present work, fuel and oxidizer were hydrogen and oxygen. However, in contrast to [4], where calculations were performed for homogeneous stoichiometric hydrogen–air mixture, in the present work, we considered a separate supply of the components in the RDC. As in [4], the oxidation of hydrogen was described by a single-step reaction scheme:

$$H_2 + H_2 + O_2 = H_2O + H_2O. \quad (1)$$

The rate of hydrogen oxidation at elevated pressures P (5 to 40 atm) and temperatures T (1100–2000 K) was calculated by the formula

$$[\dot{H}_2] = -8.0 \cdot 10^{11} P^{-1.15} [H_2]^2 [O_2] e^{-10^4/T} \quad (2)$$
$$(\text{atm, mol, L, s}).$$

This formula was obtained by fitting the dependences of the induction period on the pressure and tempera-

ture obtained for scheme (1) to those calculated within the framework of an extensively tested detailed kinetic mechanism of hydrogen oxidation [15]. Note that the heat of reaction (1) was modified so at make the calculated Chapman–Jouguet detonation velocity D_{CJ} for stoichiometric hydrogen–air mixture be consistent with its thermodynamic value ($D_{CJ} \approx 1970$ m/s).

The boundary conditions for the average flow velocity, pressure, temperature, turbulent kinetic energy and its dissipation rate and mean concentrations of chemical components on the solid walls of the RDC were set using the formalism of wall functions on the assumption that the walls are isothermal (T_w = 293.15 K), impermeable, and noncatalytic, with no-slip properties.

At the entrances to the air (subscript a) and hydrogen (subscript f) the collectors of the RDC, the inlet boundary conditions in the form of fixed values of the pressure, temperature, turbulent kinetic energy and its dissipation rate, and the average concentrations of oxidant and fuel, respectively, were specified.

The outlet of the RDC was connected to a receiver with a volume many times greater than the RDC volume. At the boundaries of the receiver, the von Neumann condition, grad(P) = 0, was set. The rest of the variables (velocity, temperature, turbulent kinetic energy and its dissipation rate, and the concentrations of components) were extrapolated to these boundaries from the computational domain. Special calculations demonstrated that the specified boundary conditions at the receiver boundaries produce no effect whatsoever on the solution.

The boundary conditions for the particles (the components of the velocity vector and scalar variables) on the solid walls of the RDC and the open boundaries of the computational domain were formulated in such a way that they would be consistent with the boundary conditions for the mean values of the relevant variables. This consistency was continuously monitored by comparing the values of the variables obtained by averaging over the ensemble of particles in the computational mesh with the average values of the same variables obtained by solving the averaged equations of flow.

The initial conditions for the average parameters of the flow were formulated as follows. It was assumed that, at initial time $t = 0$, the air and hydrogen collectors are filled with air and hydrogen under static pressures P_a and P_f, respectively, and the rest of the region is filled with quiescent air at atmospheric pressure.

The initial positions of the particles in the computational domain were selected using a random number generator capable of providing an on-average uniform distribution over a unit-length interval. At the initial time, each particle was characterized by a set of specific values of all relevant variables consistent with the initial distributions of the corresponding average values. The nominal number of particles in the computational mesh P_e was specified before simulation, $N_p = 10$. Note that, in the process of computations, the actual number of particles in the meshes could change (particles migrated over the computational domain). To keep the number of particles unchanged, special procedures of cloning and clustering were applied.

The pattern of the flow in the RDC was generally dependent on the chosen value of N_p and on the computational grid. However, preliminary calculations showed that, at $N_p > 10$–15, the dependence of the flow pattern on N_p becomes weak. The influence of the computational grid was investigated by comparing the results of calculations on different grids, containing 1.5 million and 5 million meshes. As regards the internal structure of the detonation front, the computational grids used did not allow resolving it adequately. The last will be the subject of further studies.

The calculation procedure was started with purging the RDC for 0.4 ms, a time long enough to form a 10-cm-thick active layer of hydrogen–air mixture over the RDC bottom. Then, the procedure of detonation initiation was performed. This procedure amounts to a rapid burning of particles located in the initiator region, a limited-size area in the active layer. The combustion of the particles rapidly raises the pressure in the initiator region, thereby forming a shock wave. To ensure the propagation of the detonation wave (DW) in the desired direction, for example, counterclockwise, the initial distribution of particles in the RDC in the clockwise direction from the initiator region contained a layer of temporarily inert particles. Immediately after the initiation of detonation, these particles become active.

Figure 2 shows the experimental curves of the pressure in the air and hydrogen collectors and the parameters of the two variants of calculations discussed below. In the experiments described in [5, 6], a continuous supply of the components of the combustible mixture was provided using finite-volume receivers, so the pressure in the collectors decreased during the experiment. In our calculations, the pressures in the air and hydrogen collectors were considered constant (indicated by points in the experimental curves). Variant 1, with pressures in the air and hydrogen collectors of $P_a = 6$ atm and $P_f = 37$ atm, corresponds to the initial conditions of the experiments in [5, 6]. Variant 2 was selected to study the effect of pressure in the hydrogen collector (P_f = 18.5 atm) on the performance characteristics of the RDC.

CALCULATION RESULTS

In Fig. 3 shows the calculated instantaneous distributions of pressure (a), temperature (b), and the mass fractions of hydrogen (c) and oxygen (d) near the outer wall of the RDC for variant 1 at time $t = 5.7$ ms. In addition to Fig. 3, Fig. 4 shows the calculated instantaneous distribution of the same parameters at the same time and for the same variant, but at the $z = 40$ mm cross-

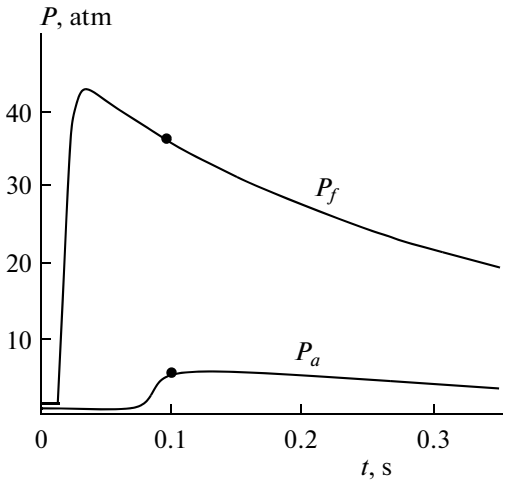

Variant no.	1	2
P_a, atm	6	6
P_f, atm	37	18.5

Fig. 2. Experimental curves of pressure in the air P_a and hydrogen P_f collectors. The parameters of the two variants of calculations are given below.

section. In contrast to the currently available models of RDC operation, the model underlying the present calculations takes into account the possibility of micromixing of gases and chemical transformations in the zones of mixing of detonation products with fresh components of the combustible mixture. Figures 3 and 4 show that the DW propagates through a substantially inhomogeneous medium, with variable temperature and chemical composition. Variant 1 provides a stable operation of the RDC with one DW, which becomes periodic ~3 ms after initiation. Interestingly, the experiments described in [5, 6] also demonstrated the onset of the periodic mode of rotating detonation at a time of ~3 ms after initiation. The calculated rotation frequency of the DW turned out to be ~123000 rpm (2.0–2.1 kHz). The height of the layer of hydrogen–air mixture directly ahead of the DW (Figs. 3c, 3d) was ~100–150 mm, in agreement with the experimental value [5, 6].

Note, however, that, in contrast to our calculations, the experiments performed in [5, 6] demonstrated the existence of not one but two or even three DWs simultaneously propagating over the RDC bottom, approximately equidistant from each other. A careful analysis of the calculation results revealed that the structure of the flow behind the DW is indicative of periodically occurring well-pronounced supersonic reaction fronts (one, two, or more). For example, Figs. 5a and 5b show situations where the DW (designated by 1) has no additional reaction fronts behind (Fig. 5a) and where there are three additional reaction fronts (*2–4* in Fig. 5b). The intensities of these fronts are lower than that of the detonation front, so we were forced to change the pressure scale in Figs. 5a and 5b. For a quantitative analysis of the reaction front, consider Fig. 6, which shows an example of calculated time dependences of the static pressure and static temperature at a point on the outer wall near the RDC bottom. It is seen that, in the intervals between the major peaks of pressure and temperature, corresponding to the DW, lower-intensity peaks associated with additional reaction fronts manifest themselves. The question of why these fronts are not transformed in calculations into detonation waves remains open. Possible explanations include the use of a simplified model of molecular mixing and a simplified one-step kinetic scheme of hydrogen oxidation.

Figure 7 shows the calculated time dependence of the DW velocity for two variants: 1 (Fig. 7a) and 2 (Fig. 7b), with the DW velocity on the external D_{ext} (solid lines) and the internal D_{int} (dashed lines) walls of the RDC. The DW velocity was defined as $D = \Delta L/\Delta t$, where ΔL is the path (arc length) traversed by the wave in a time interval Δt. The DW front coordinate was determined from the position of the highest pressure peak. Figure 7 shows that, in both cases, the DW velocity along the outer wall is higher than along the inner. This issue requires further discussion.

First, a steady propagation of the DW is possible only if the local instantaneous conditions ahead of the wave front (the thermodynamic state and gas mixture composition) are maintained at a constant level and within the parametric domain of existence of detonation. Therefore, in general, the velocities D_{ext} and D_{int} are determined by the processes of mixing the fuel components with each other and with the detonation products of the previous cycle, as well as by the diffraction of the DW at the chamber walls and the lateral expansion of the products.

Second, to ensure steady (on average) detonation propagation in an annular channel, it is necessary to satisfy the condition

$$D_{ext}/D_{int} \approx 1 + 2\Delta/d_{int}. \quad (3)$$

This condition is easy to obtain by assuming that the front of the DW on average retains its shape. In accordance with this condition, for the given RDC design, the ratio $D_{ext}/D_{int} \approx 1.18$ should hold, which is in satisfactory agreement with the data presented in Figs. 7a and 7b. Thus, in the steady periodic mode, the system of supply of the gas mixture components into the RDC should provide such a thermodynamic state and a composition of the mixture in ahead of the DW at which the velocities D_{ext} and D_{int}, on the one hand, occur within the parametric domain of existence of detonation in an RDC of a given size and, on the other, satisfy geometric condition (3).

Figure 8 demonstrates the structure of the flow near the bottom of the RDC operating in the periodic

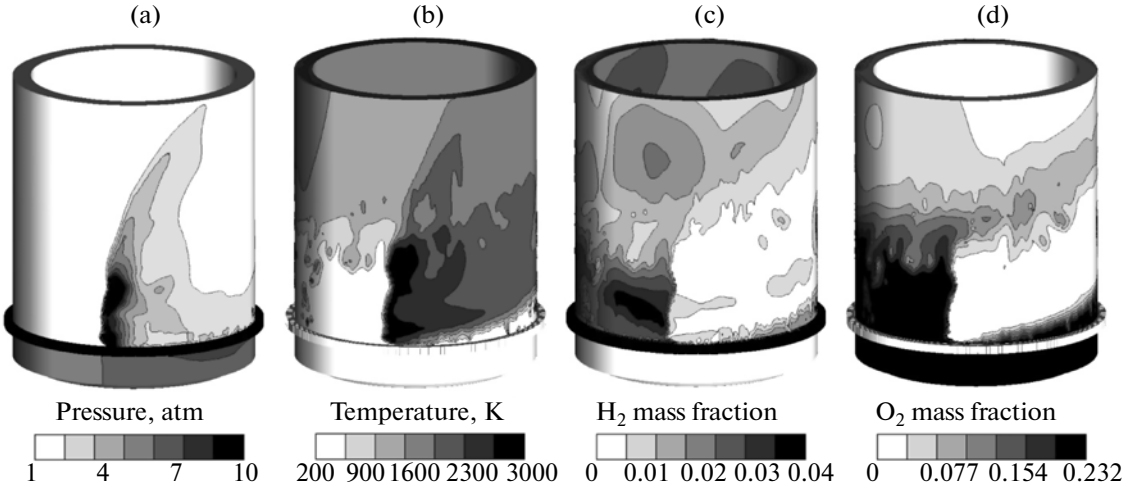

Fig. 3. Instantaneous distributions of (a) pressure, (b) temperature, and (c) hydrogen and (d) oxygen mass fractions, near the external wall of an RDC operating in the mode of separate supply of air and hydrogen. Detonation propagates from the right to the left. Variant 1.

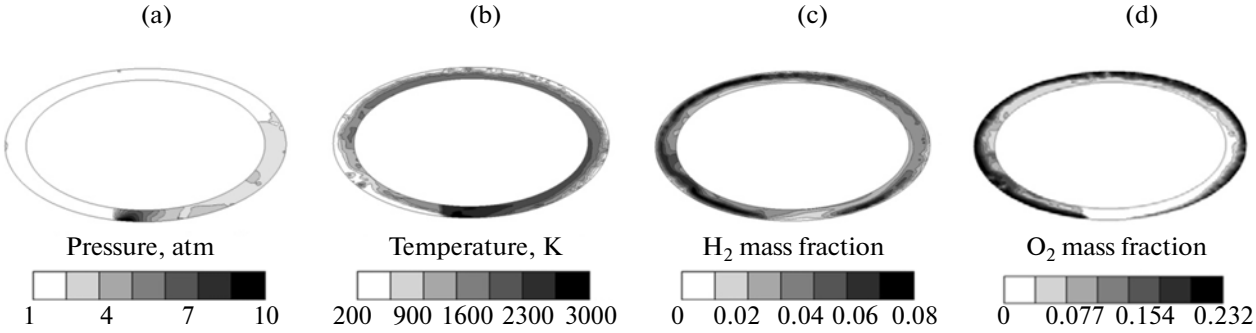

Fig. 4. Instantaneous distributions of (a) pressure, (b) temperature, and (c) hydrogen and (d) oxygen mass fractions at a cross section $z = 40$ mm from the RDC bottom. Detonation propagates from the right to the left. Variant 1.

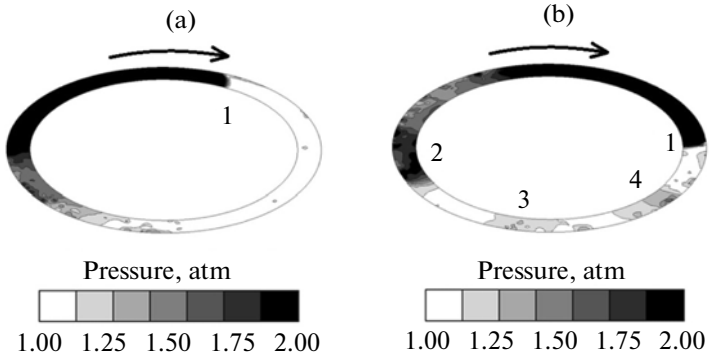

Fig. 5. Instantaneous distributions of (a) pressure, (b) temperature, and (c) hydrogen and (d) oxygen mass fractions at a cross section $z = 40$ mm from the RDC bottom at times $t =$ (a) 2.90 and (b) 6.86 ms, when only one detonation wave (1) propagates, without other supersonic reaction fronts (a) and when there are three additional reaction fronts (2, 3, 4) (b). Detonation propagates clockwise. Variant 1.

mode. It shows the time evolution of the static pressure at points *1* and *2* located on the outer wall of the RDC in the $z = 40$ mm cross section 180° apart for calculation variant 1. The estimated average static pressure in this cross section (1.8 atm) was close to the experimental value, which ranged in [5, 6] from 1.8 atm (at the beginning of the experiment) to 1.2 atm (at the end).

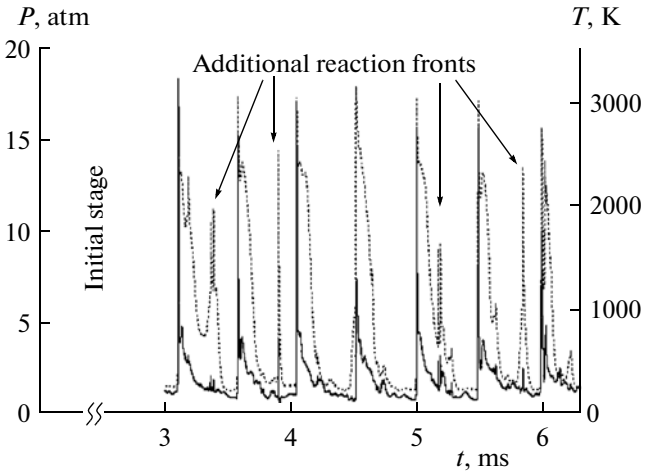

Fig. 6. Calculated time dependences of the static pressure (solid curve) and static temperature (dashed curve) at a point located at the external wall of the RDC at a distance of $z = 40$ mm from the bottom. Variant 1.

As can be seen from Fig. 8, the absolute values and pulsations of the maximum pressure in the DW front on the outside wall are much higher than on the inner. On the one hand, this is due to the different influences of the external and internal walls on the DW front [4] and, on the other, because of the pattern of mixing the combustible mixture components in the RDC. Indeed, the segment of the DW front adjacent to the outer wall undergoes reflection because of a compression action of the wall, whereas the segment adjacent to the inner wall experiences attenuation due to the expanding action of the wall. To illustrate the mixing pattern, Fig. 9 displays the calculated fields of fuel-to-oxidizer equivalence ratio, average velocity, temperature, and water vapor mass fraction~~, as well as the fuel-to-oxidizer equivalence ratio~~ at the time immediately before DW arrival. It is seen that the mixing of hydrogen and air near the outer wall ~~(Fig. 9d)~~ is much better than that near the inner wall (Fig. 9a). Moreover, in the area of reverse flows, located at the inner wall near the RDC bottom (Fig. 9b), a large amount of hot detonation products of the previous cycle accumulates (Figs. 9c, 9d).

Inspection of Fig. 9 led us to an important conclusion: in calculation variant 1, which corresponds to the initial stage of the experiments described in [5, 6], the mixing pattern is such that an incomplete combustion of hydrogen takes place: nearly one-half of the hydrogen introduced remains unburnt. This conclusion is confirmed by Fig. 10, which displays the calculated time dependences of the hydrogen mass fraction at a point in the mid cross section of the RDC $z = 350$ mm from the RDC bottom in calculation variants 1 and 2. In variant 1, the concentration of unreacted hydrogen is much higher than in variant 2, in which the pressure of fuel supply into the RDC is reduced twofold compared to variant 1.

The calculation results for variant 1 are generally consistent with the experimental data: in [~~1, 2~~], the fuel-to-oxidizer equivalence ratio was varied during the experiment from 3.34 to 0.4, whereas in our calculations, it was ~1.8. As regards variant 2, Fig. 11, like Fig. 9, shows the calculated fields of fuel-to-oxidizer equivalence ratio, velocity, temperature, and water vapor mass fraction at an instant of time immediately preceding DW arrival. A comparison of Figs. 11 and 9 suggests that the mixing of hydrogen and air in variant 2 is much better than in variant 1 (Figs. 11a and 9a). The calculated ~~statistical-average~~ pressure at the $z = 40$ mm cross section (1.47 atm) in version 2 was lower than in variant 1 (1.8 atm).

Figure 12 compares the calculated time dependence of the mass flow rates of air ~~(Fig. 12a)~~ and hydrogen ~~(Fig. 12b)~~ for variants 1 and 2. Note that the mass flow rates of air and hydrogen measured in the

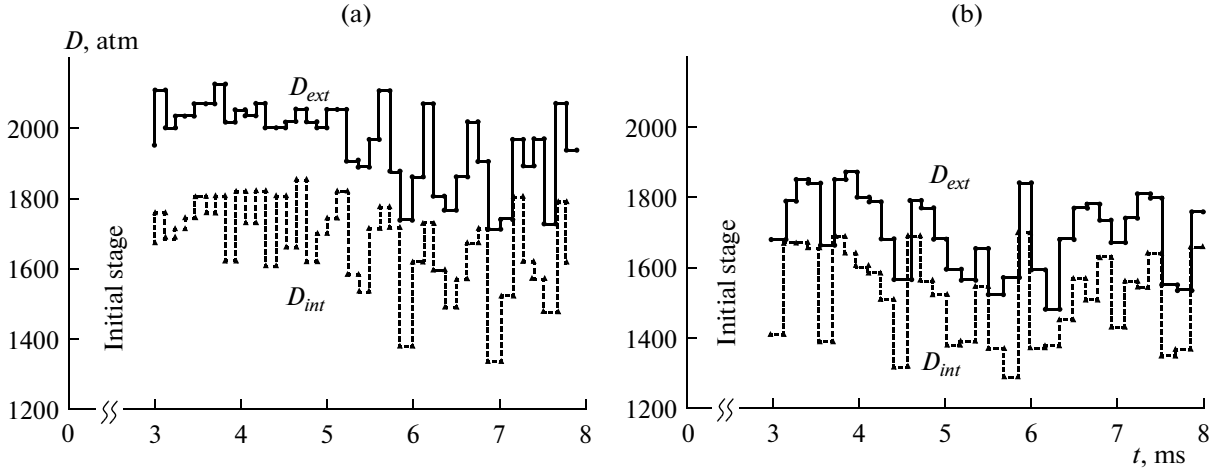

Fig. 7. Detonation velocity at the external (solid lines) and internal (dashed lines) walls of the RDC as a function of the time for variants (a) 1 and (b) 2 at a distance of $z = 40$ mm from the chamber bottom.

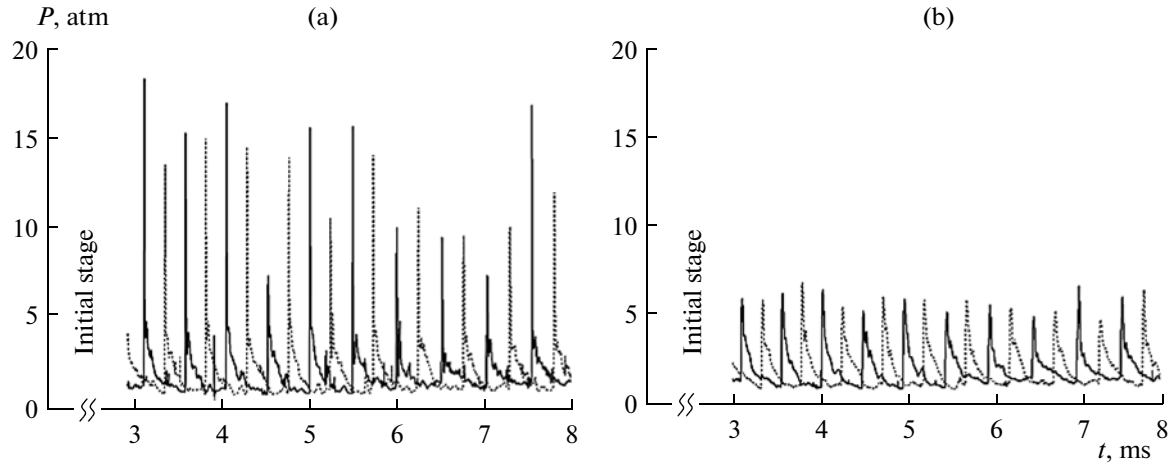

Fig. 8. Calculated time dependences of the static pressure at two points located in the RDC a distance of $z = 40$ mm from the bottom 180° apart (solid and dashed curves) at the (a) external and (b) internal walls. Variant 1.

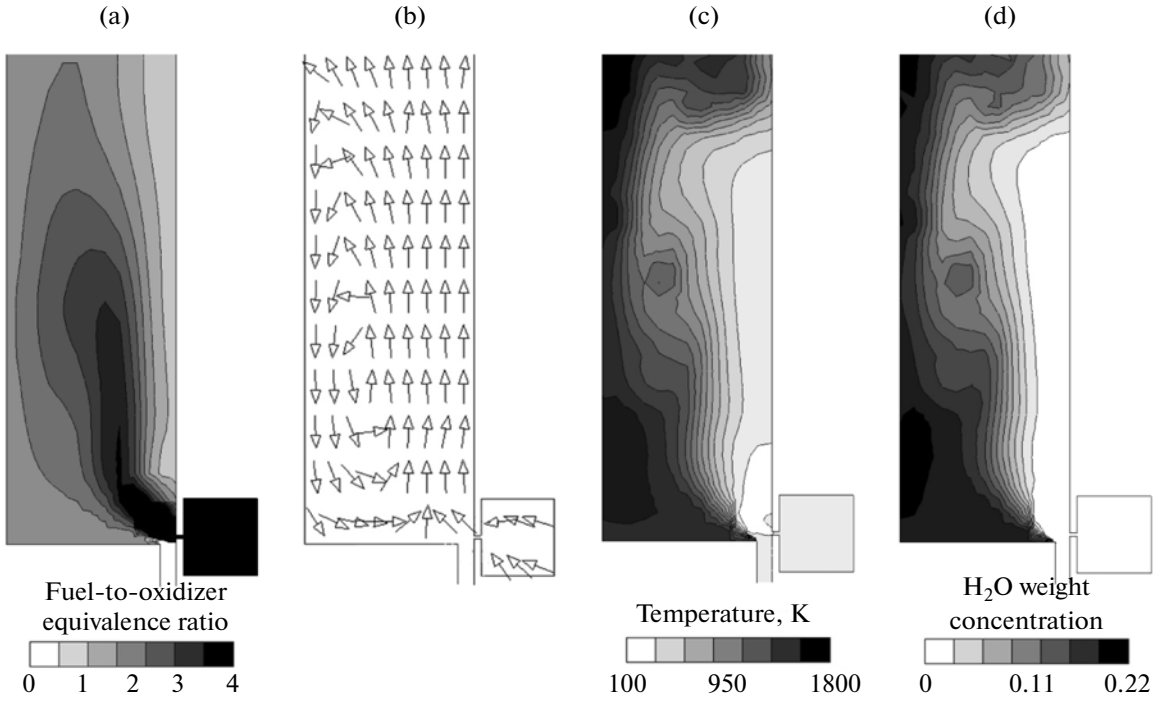

Fig. 9. Instantaneous distributions of (a) fuel-to-oxidizer equivalence ratio, (b) velocity, (c) temperature, and (d) water vapor mass fraction in the longitudinal section of the RDC at a time immediately before detonation wave arrival. Variant 1.

experiments described in [5, 6] were 1.6–4.0 and 0.07–0.28 kg/s, respectively. As can be seen from Fig. 12, at the pressures in the air and hydrogen collectors we used in variants 1 and 2, the calculated flow rates of air and hydrogen are generally in good agreement with the experimental values.

EFFECT OF GRID REFINEMENT ON THE CALCULATION RESULTS

To test how grid refinement affects the results, we performed calculations on a grid with a mesh size twice as small (mesh volume decreased eightfold) in the part of the RDC where the mixing of the combustible mixture components occurs and intense chemical reactions takes place ($0 < z < 160$ mm). Figure 13 compares the results obtained on the two different grids (conventionally termed "coarse" and "fine) containing, as noted above, 1.5 million and 5.0 million meshes, respectively. As can be seen, the flow pattern qualitatively remains unchanged, although the use of the fine grid resulted in some decrease in the DW velocity (by 6%) and changes in peak values of the

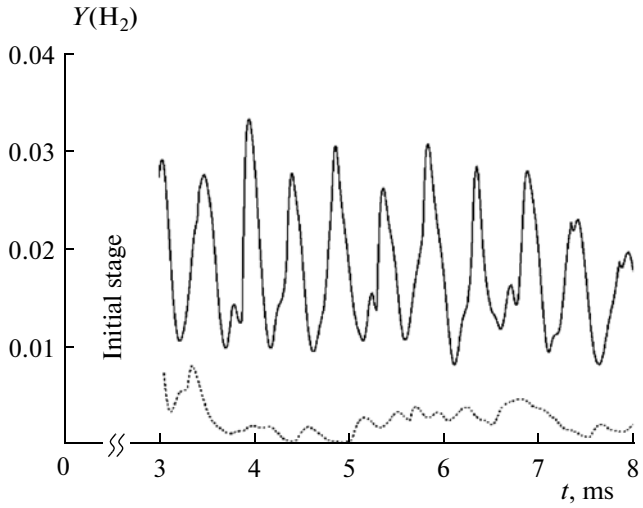

Fig. 10. Calculated time dependences of the hydrogen mass fraction at a point of middle cross section of the RDC at a distance of $z = 350$ mm from the bottom for variants 1 (solid) and 2 (dashed curve).

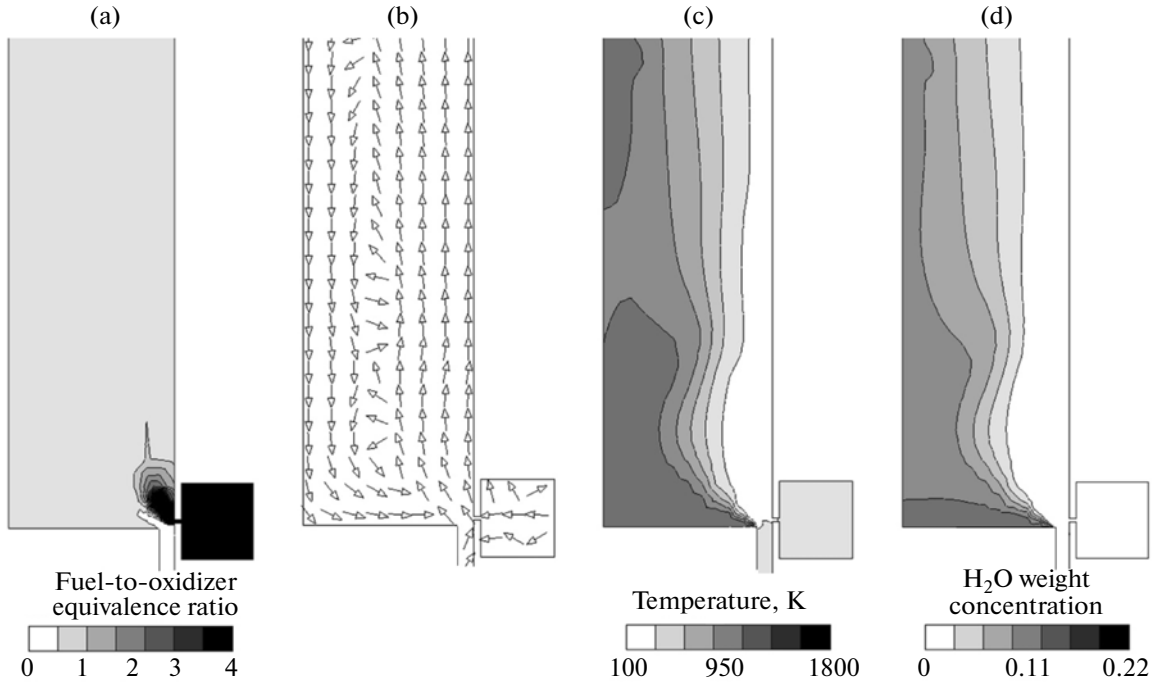

Fig. 11. Instantaneous distributions of (a) fuel-to-oxidizer equivalence ratio, (b) velocity, (c) temperature, and (d) water vapor mass fraction in the longitudinal section of the RDC at a time immediately before detonation wave arrival. Variant 2.

pressure. Nevertheless, we can claim that the results are generally valid.

CONCLUSIONS

Thus, we for the first time carried out a three-dimensional numerical simulation of the operation of an annular RDC with separate supply of the combustible mixture components, hydrogen and air, the RDC design and the main operational parameters being the same as in the experiments described in [5, 6]. The calculations were performed with allowance for the effects of finite rates of turbulent and molecular mixing of the initial components with each other and with the detonation and reaction products.

The calculation results were compared to the experimental data obtained at Lavrentyev Institute of Hydrodynamics of the Siberian Branch of the Russian Academy. The estimated height of the layer of hydrogen–air mixture immediately ahead of the DW propagating through a significantly inhomogeneous 3

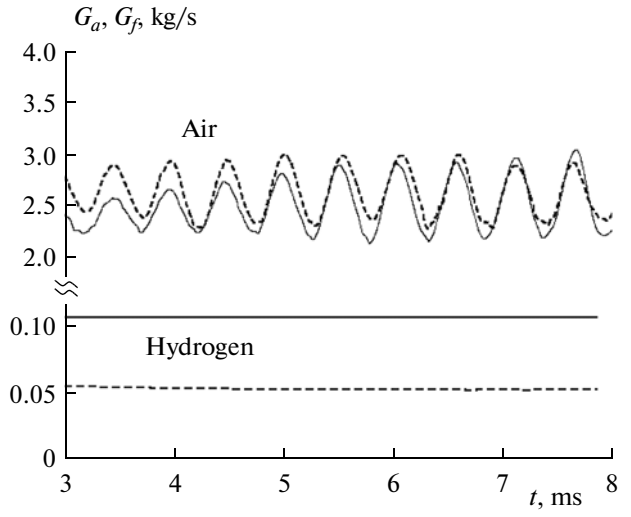

Fig. 12. Comparison of the calculated time dependences of the mass flow rates of air and hydrogen for variants 1 (solid curve) and 2 (dashed).

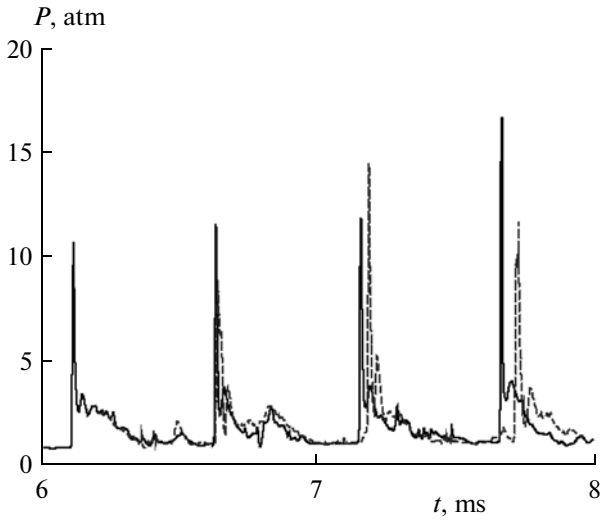

Fig. 13. Comparison of the calculated time dependences of the static pressure at a point located at the external wall of the RDC at a distance of $z = 40$ mm for the coarse (solid curve) and fine (dashed) computational grid. Variant 1.

medium with variable temperature and chemical composition was ~100–150 mm, close to the value measured in [5, 6]. In contrast to these experiments, in which two or three DWs traveling over the RDC bottom were observed, the calculations under the same conditions predict stable operation mode with one DW. However, a careful analysis of the calculation results showed that the flow structure behind the DW features periodically arising supersonic reaction fronts (one, two or more), which are not transformed into detonation waves. These discrepancies between the calculation results and experimental data require further studies.

ACKNOWLEDGMENTS

This work was supported in part by the program of the Presidium of RAS no. 26 “Combustion and Explosion” and the Russian Foundation for Basic Research (project no. 11-08-01297).

REFERENCES

1. Ya. B. Zel’dovich, Zh. Tekh. Fiz. **10** (17), 1453 (1940).
2. B. V. Voitsekhovskii, Sov. Phys. Dokl. **4**, 1207 (1959).
3. *Pulse Detonation Motors*, Ed. by S. M. Frolov (Torus Press, Moscow, 2006) [in Russian].
4. S. M. Frolov, A. V. Dubrovskii, and V. S. Ivanov, Russ. J. Phys. Chem. B **6**, 276 (2012).
5. F. A. Bykovskii, S. A. Zhdan, and E. F. Vedernikov, Fiz. Goreniya Vzryva **42** (4), 1 (2006).
6. F. A. Bykovskii, S. A. Zhdan, and E. F. Vedernikov, Combust. Explos., Shock Waves **46**, 52 (2010).
7. D. Schwer and K. Kailasanath, Proc. Combust. Inst. **33**, 2195 (2011).
8. M. Hishida, T. Fujiwara, and P. Wolanski, Shock Waves **19** (1), 10 (2009).
9. S. B. Pope, Prog. Energy Combust. Sci. **11**, 119 (1985).
10. S. M. Frolov, V. Ya. Basevich, M. G. Neuhaus, and R. Tatschl, in *Advanced Computation and Analysis of Combustion*, Ed. by G. D. Roy, S. M. Frolov, and P. Givi (ENAS, Moscow, 1997), p. 537.
11. S. M. Frolov and V. S. Ivanov, in *Deflagrative and Detonative Combustion*, Ed. by G. D. Roy and S. M. Frolov (Torus Press, Moscow, 2010), p. 133.
12. V. S. Ivanov and S. M. Frolov, Russ. J. Phys. Chem. B **5**, 597 (2011).
13. S. Patankar, *Numerical Methods of Solution of Problems of Heat Transfer and Dynamics of Liquid* (Hemisphere, New York, 1980; Energoatomizdat, Moscow, 1984).
14. S. M. Frolov, V. S. Ivanov, B. Basara, and M. Suffa, J. Loss Prevention Process Industr. (2011). doi:10.1016/j.jlp.2011.09.007.
15. V. Ya. Basevich and S. M. Frolov, Russ. Chem. Rev. **76**, 867 (2007).

SPELL: 1. preflame, 2. unburnt, 3. inhomogeneous